Acta Biomaterialia xxx (xxxx) xxx

Contents lists available at ScienceDirect

Acta Biomaterialia

journal homepage: www.elsevier.com/locate/actbio

Polymeric nanoparticles functionalized with muscle-homing peptides for targeted delivery of phosphatase and tensin homolog inhibitor to skeletal muscle

Di Huang[a,b,c], Feng Yue[a,*], Jiamin Qiu[a], Meng Deng[b,c,d,e], Shihuan Kuang[a,f,*]

[a] Department of Animal Sciences, Purdue University, West Lafayette, IN, USA
[b] Department of Agricultural and Biological Engineering, Purdue University, West Lafayette, IN, USA
[c] Bindley Bioscience Center, Purdue University, West Lafayette, IN, USA
[d] School of Materials Engineering, Purdue University, West Lafayette, IN, USA
[e] Weldon School of Biomedical Engineering, Purdue University, West Lafayette, IN, USA
[f] Center for Cancer Research, Purdue University, West Lafayette, IN, USA

ARTICLE INFO

Article history:
Received 25 June 2020
Revised 1 October 2020
Accepted 7 October 2020
Available online xxx

Keywords:
Duchenne muscular dystrophy
PTEN signaling
Polymeric nanoparticles
Targeted drug delivery
Muscle-homing peptides

ABSTRACT

Phosphatase and tensin homolog (PTEN) antagonizes muscle growth and repair, and inhibition of PTEN has been shown to improve the pathophysiology and dystrophic muscle function in a mouse model of Duchenne muscular dystrophy (DMD). However, conventional pharmacological delivery of PTEN inhibitors carries a high risk of off-target side effects in other non-muscle organs due to broad targeting spectrums. Here we report a muscle-targeted nanoparticulate platform for cell-specific delivery of a PTEN inhibitor. Poly(lactide-*co*-glycolide)-*b*-poly(ethylene glycol) nanoparticles (NPs) are functionalized with a muscle-homing peptide M12 to promote the selective uptake by muscle cells/tissue *in vitro* and *in vivo*. Moreover, the NPs are formulated to slowly release the PTEN inhibitor, preventing cytotoxicity associated with direct exposure to the drug and facilitating sustained inhibition of PTEN. This advanced delivery approach taking advantages of polymeric nanomaterials and muscle-homing peptides opens a new avenue for the development of long-term therapeutic strategies in DMD treatment.

Statement of Significance

Pharmacological inhibition of phosphatase and tensin homolog (PTEN) has been demonstrated to improve muscle function in a mouse model of Duchenne muscular dystrophy (DMD), but translation of this approach into clinical settings remains challenging due to potential risks of off-target side effects. Herein, we developed a nanoparticulate platform, consisting of poly(lactide-*co*-glycolide)-*b*-poly(ethylene glycol) and a muscle-homing peptide M12, for cell-specific delivery of a PTEN inhibitor. M12 facilitates the cellular internalization of nanoparticles in myoblasts and their selective localization in skeletal muscle. Moreover, the slowly released drug from nanoparticles reduces its cytotoxicity and achieves sustained PTEN inhibition. This advanced delivery approach taking advantages of nanomaterials and targeting peptides opens a new avenue for the development of long-term therapeutic strategies in DMD treatment.

1. Introduction

Duchenne muscular dystrophy (DMD), a X-linked disorder and the most common inherited muscle disease of early childhood, occurs in 1 out of 5000 male births [1]. It results in muscle degeneration, severe physical disability, and premature fatality. DMD is caused by mutations in the DMD gene, which encodes a protein called dystrophin. Dystrophin localizes to the sarcolemma of skeletal muscle, forming one component of the dystrophin-associated glycoprotein complex, and acts as a mechanical link between the muscle fiber cytoskeleton and extracellular matrix [2,3]. Mutations in the DMD gene cause the deletion of certain regions of the dystrophin gene and the production of a dysfunctional dystrophin protein. The lack of functional dystrophin in DMD patients disrupts the dystrophin-associated glycoprotein complex in myofibers,

* Corresponding author.
E-mail addresses: fyue@purdue.edu (F. Yue), skuang@purdue.edu (S. Kuang).

https://doi.org/10.1016/j.actbio.2020.10.009
1742-7061/

thereby rendering the muscle fibers less resistant to mechanical stress during muscle contractions [4,5].

Gene therapy has long been considered a promising option for the treatment of DMD due to the genetic nature of this disease. However, the large size of the dystrophin cDNA poses a challenge to delivery. Consequently, several therapeutic strategies aim to ameliorate dystrophic pathophysiology by targeting signaling pathways that control skeletal muscle growth, including matrix metalloproteinase-9 [6], insulin-like growth factor-1 [7,8], forkhead box protein O1 [9], and myostatin [10]. Phosphatase and tensin homolog (PTEN) is a dual-specificity lipid and protein phosphatase that dephosphorylates phosphatidylinositol-3,4,5-trisphosphate (PIP3) to phosphatidylinositol-4,5-bisphosphate (PIP2), thereby negatively regulating the phosphoinositide 3-kinase (PI3K)-dependent signaling pathway [11]. The substantially elevated expression of PTEN has been detected in skeletal muscle of DMD patients and animal models with pathological features of DMD [12,13]. The PTEN signaling has therefore been considered a potential therapeutic target to treat DMD.

Our previous studies have shown that genetic deletion of *Pten* restores the integrity of muscle basement membrane and prevents the degeneration of dystrophic myofibers in the *mdx* mouse model of DMD [14]. More importantly, pharmacological inhibition of PTEN by intraperitoneal administration of VO-OHpic trihydrate, a potent inhibitor of PTEN, improves the pathophysiology and dystrophic muscle function of *mdx* mice. However, translation of this approach into clinical settings for DMD treatment remains challenging due to the potential risks resulting from broad targeting spectrums that affect multiple organs or tissues. Moreover, the short half-life of PTEN inhibitors ($<$ 2 days) induced by hydrolysis necessitates frequent injections, causing patient compliance issues [15,16].

To overcome these limitations of therapeutic agents delivered in native forms, nanoparticle (NP)-mediated delivery is considered an encouraging strategy. Drug molecules can be encapsulated into NPs, which offer both temporal and spatial control of drug release, thereby substantially reducing the frequency of administration. NPs based on biodegradable, biocompatible, and FDA-approved polymers are of interest. The use of polymers with good clinical track record facilitates the future translation of NP formulations into clinical trials. Poly(lactide-*co*-glycolide) (PLGA) NPs as the controlled release system are a desirable option due to their well-established safety profile in clinic [17]. Poly(ethylene glycol) (PEG)-functionalized PLGA NPs are particularly promising, since PEGylated polymeric NPs exhibit significantly reduced systemic clearance and prolonged circulating half-life compared to the particles without PEGylation [18]. Moreover, PEGylation has been shown to improve the efficacy, safety, and patient compliance of various FDA-approved drugs in the clinical practice [19].

Another unique advantage of NPs in therapy is their ability to actively target the cells or tissues of interest through surface engineering. Active targeting involves utilizing affinity ligands on the surface of NPs for enhanced retention and uptake by the target cells. To that end, ligands are selected to bind surface molecules or receptors specifically expressed in the target cells or tissues and they need to be in the proximity of their targets to benefit from this increased binding affinity [20]. Therefore, the approach is aimed toward increasing interactions between NPs and cells as well as enhancing cellular internalization of the encapsulated drug without largely altering the overall *in vivo* properties [21]. Some targeted NP delivery systems have shown considerable clinical benefits in cancer therapy and great scope for further improvement [22,23]. By screening, Gao et al. has previously identified a muscle-homing peptide M12 (RRQPPRSISSHP) that preferentially binds to biologically active molecules or receptors present on the surface of muscle cells [24]. Repeated administration of peptide conjugates could improve the delivery efficiency of phosphorodiamidate morpholino oligomers and the muscle function [24–26], showing great potential for serving as an actively targeted ligand to enhance the specificity and efficiency of NP-mediated drug delivery to skeletal muscle.

Herein, we describe polymeric NPs functionalized with a targeting peptide for enhanced and site-specific delivery of a PTEN inhibitor to skeletal muscle. This NP delivery system consists of a hydrophobic PLGA core encapsulating with a PTEN inhibitor VO-OHpic trihydrate, a hydrophilic PEG shell, and muscle-homing peptide M12 ligands. PLGA-PEG NPs functionalized with M12 greatly increase the cellular uptake efficiency of NPs in myoblasts *in vitro* and their localization in skeletal muscle *in vivo*, potentially allowing enhanced therapeutic efficacy and bypassing unwanted off-target side effects. Also, slowly released VO-OHpic trihydrate from NPs reduces its cytotoxicity and achieves sustained PTEN inhibition, which would improve long-term treatment outcomes. This design rationale has produced promising results through taking advantages of muscle-targeted nanomedicine coupled with inhibition of PTEN signaling, opening new avenues for the development of therapeutic strategies in DMD treatment.

2. Materials and methods

2.1. Materials

Methoxy poly(ethylene glycol)-*b*-poly(lactic-*co*-glycolic acid) (mPEG-PLGA; Mw 5000-20,000 Da; 50:50 La:Ga (w:w); Cat. #AK037), Poly(lactide-*co*-glycolide)-*b*-poly(ethylene glycol)-N-hydroxysuccinimide (PLGA-PEG-NHS; Mw 20,000-5000 Da; 50:50 La:Ga (w:w); Cat. #AI111), and Poly(lactide-*co*-glycolide)-*b*-poly(ethylene glycol)-amine (PLGA-PEG-NH_2; Mw 20,000-5000 Da; 50:50 La:Ga (w:w); Cat. #AI188) were purchased from PolySciTech (West Lafayette, IN, USA). VO-OHpic trihydrate (Mw 415.20; Cat. #S8174) was obtained from Selleck Chemicals (Houston, TX, USA). M12 peptide (RRQPPRSISSHP, Mw 1417.6) was purchased from Thermo Fisher Scientific (Waltham, MA, USA). Nile red (Mw 318.4; Cat. #151744) and Alexa Fluor® 488 NHS ester (Mw 732.74; Cat. #41820) were purchased from MP Biomedicals (Solon, OH, USA) and Lumiprobe Corporation (Hunt Valley, MD, USA), respectively. Polyvinyl alcohol (PVA, 87%-90% hydrolyzed; Mw 30-70 kDa) and anti-Laminin antibody (Cat. #L9393) were obtained from Sigma-Aldrich (St. Louis, MO, USA). Goat polyclonal secondary antibody to rabbit immunoglobulin G (IgG) - H&L (DyLight® 594, Cat. #ab96901) was obtained from Abcam (Cambridge, UK). AKT (pan) (40D4) (Cat. #2920), phospho-AKT (Ser473) (D9E) (Cat. #4060), S6 ribosomal protein (5G10) (Cat. #2217), and phospho-S6 ribosomal protein (D57.2.2E) (Cat. #4858) antibodies as well as horseradish peroxidase (HRP)-conjugated secondary antibodies, including anti-rabbit immunoglobulin G (IgG) (Cat. #7074S) and anti-mouse IgG (Cat. #7076S), were purchased from Cell Signaling Technology (Danvers, MA, USA). CellTiter 96® AQ_{ueous} one solution reagent containing a tetrazolium compound [3-(4,5-dimethylthiazol-2-yl)-5-(3-carboxymethoxyphenyl)-2-(4-sulfophenyl)-2H-tetrazolium, inner salt; MTS] was purchased from Promega (Madison, WI, USA). β-Actin (Cat. #SC-47778) antibody was purchased from Santa Cruz Biotechnology (Dallas, TX, USA). All the organic solvents used in experiments were purchased from Thermo Fisher Scientific (Waltham, MA, USA). All other reagents were purchased from Sigma-Aldrich (St. Louis, MO, USA).

2.2. Animals

Animals were housed at a density of up to five males or five females per cage under specific pathogen-free conditions in the animal facility with free access to water and standard rodent chow food. Room temperature was maintained at a temperature

Please cite this article as: D. Huang, F. Yue, J. Qiu et al., Polymeric nanoparticles functionalized with muscle-homing peptides for targeted delivery of phosphatase and tensin homolog inhibitor to skeletal muscle, Acta Biomaterialia, https://doi.org/10.1016/j.actbio.2020.10.009

of 18-23°C with a 12-h light/12-h dark cycle and 40-60% humidity. D2.B10-*Dmd*^{mdx}/J mice (D2-*mdx*; JAX Stock #013141) were purchased from Jackson Laboratory (Bar Harbor, ME, USA) and 2-month-old mice were used in the experiments. All animal procedures were approved by the Purdue University Animal Care and Use Committee.

2.3. Preparation and characterization of NPs

NPs were formulated using the emulsion solvent evaporation technique. Briefly, 10 mg of copolymers mPEG-PLGA and PLGA-PEG-NHS (1:1 w/w) were dissolved in a mixture of dichloromethane and dimethylformamide (4:1 v/v) with or without a predefined amount of drug compounds, including VO-OHpic or Nile red. A volume of 1 mL of polymer/drug solution was added into 3 mL of aqueous phase containing 1% PVA, followed by probe sonification (Sonic Dismembrator Model 100, Thermo Fisher Scientific, Waltham, USA) to form the emulsion. The emulsified mixture was subsequently poured into 15 mL of deionized water and stirred for 2 h at room temperature to allow solvent evaporation. The resulting NP fractions were purified by repeated centrifugation at 13,000 rpm for 50 min at 4°C (Centrifuges 5804 R, Eppendorf, Hamburg, Germany) and resuspended in deionized water. For peptide conjugation, 0.625 mg of peptide was added to a NP suspension at a concentration of 10 mg/mL, buffered by 1 M sodium bicarbonate solution to pH 8.3, and stirred overnight at 4°C. The remaining free molecules were removed by centrifugation and washing NPs for three times.

The particle size, size distribution, and zeta potential were determined by dynamic light scattering using a Malvern Nano ZS (Malvern Instruments, Worcestershire, U.K.). Samples for transmission electron microscopy were stained with an aqueous solution of 1% phosphotungstic acid and observed for size and morphology using a Tecnai G2 20 TEM (FEI Company, Hillsboro, OR, USA) at an accelerating voltage of 200 kV. The content of VO-OHpic in NPs was analyzed by a microplate reader (Synergy H1, Biotek Instruments, Winooski, VT, USA) at a wavelength of 302 nm. Drug loading is defined as the mass fraction of drug in NPs and encapsulation efficiency is the fraction of initial drug that is encapsulated by NPs.

2.4. Drug release from NPs

To determine the release kinetics, a suspension of VO-OHpic loaded NPs at a concentration of 10 mg/mL was placed into a semipermeable dialysis bag (MWCO 12-14 kDa; Spectrum Labs, San Francisco, CA, USA) and immersed in 10 mL of 0.2% tween 80 in phosphate-buffered saline (PBS, pH 7.4) at 37°C with gentle agitation at 140 rpm using an orbital water bath shaker (New Brunswick Scientific, Edison, NJ, USA). Samples of medium outside the dialysis bag were collected at predetermined time points to measure the concentration of VO-OHpic using a microplate reader as described above. After sampling, the release medium was replaced with fresh buffer solution to maintain sink conditions. The concentration of VO-OHpic released from NPs was expressed as the cumulative percentage of the total drugs in NPs and plotted as a function of time.

2.5. Cell culture and cellular uptake of NPs

C2C12 myoblasts, 3T3-L1 preadipocytes, and human skeletal myoblasts were cultured in Dulbecco's modified Eagle medium (DMEM) supplemented with 10% fetal bovine serum and 1% antibiotics (penicillin and streptomycin) at 37°C, 5% CO_2, and 95% relative humidity.

C2C12 myoblasts, 3T3-L1 preadipocytes, and human skeletal myoblasts were seeded onto 12-well plates at a density of 5×10^4 cells per well and cultured for 24 h. After washing with PBS, cells were incubated with DMEM containing Nile red encapsulated NPs at a final concentration of 0.1 mg/mL for 1 h. Subsequently, cell nuclei were stained with Hoechst 33342 (1 μg/mL in PBS) at for 10 min at 37°C following by repeated washing with PBS to remove remaining NPs and dead cells. Fluorescent images were captured using a CoolSnap HQ charge coupled-device camera (Photometrics, Tucson, AZ, USA) equipped on a Leica DM 6000B microscope (Leica Camera, Wetzlar, Germany) with a $\times$ 20 objective. Cells without any NP treatment were used as negative control. For competitive inhibition studies, C2C12 myoblasts and 3T3-L1 preadipocytes were preincubated with free M12 solution in DMEM at a concentration of 50 μM for 1 h at 37°C, followed by the same procedure as described above. The corrected total cell fluorescence was quantified by measuring integrated density with background subtraction using ImageJ software. 200-300 cells in total from three individual repeats were analyzed for each group.

2.6. Preparation of fluorescent AF 488 conjugated NPs

The conjugation of AF 488 NHS ester and PLGA-PEG-NH_2 was performed by mixing 4.69 mg of AF 488 NHS ester and 20 mg of PLGA-PEG-NH_2 in 1 mL of dimethylformamide and stirring overnight at room temperature in darkness. After the reaction, the final product was precipitated with cold diethylether/methanol (1:1 v/v). The pellet was centrifuged and redissolved in dimethylformamide followed by repeated precipitation/wash cycles to remove unreacted molecules. The resulting copolymer was dried under vacuum for 24 h at room temperature. Fluorescent AF 488 conjugated NPs (AF488-PLGA-PEG NPs and AF488-PLGA-PEG-M12 NPs) were prepared following the standard protocol described above.

2.7. Biodistribution of NPs

Fluorescent AF 488 conjugated NPs (AF488-PLGA-PEG NPs or AF488-PLGA-PEG-M12 NPs) with a single dose of 80 mg/kg body weight were injected via the tail vein (intravenous injection) into *mdx* mice. Mice were anesthetized with Ketamine administered by intraperitoneal injection at 6 h post injection. Hairs on both hindlimbs were removed and the exposure parameters were adjusted using a control mouse without any treatment to avoid background autofluorescence. Images were taken with the Ami optical imaging system (Spectral Instruments Imaging, Tucson, AZ). After whole-body scanning (6 h post injection), mice were immediately euthanized and multiple tissues, including the liver, kidney, spleen, heart, quadriceps, gastrocnemius, and diaphragm, were collected, followed by the *ex vivo* imaging. The fluorescent images were analyzed by the Living Image Software and quantification of fluorescence ratio of muscle to liver was performed by dividing the fluorescence intensity of liver with that of each muscle tissue.

2.8. Immunofluorescence staining

The dissected gastrocnemius muscle tissues were embedded in optimal cutting temperature compound and frozen in isopentane that was chilled in liquid nitrogen. Cross-sections of 10 μm thickness were cut using a Leica CM1850 cryostat microtome (Leica, Wetzlar, Germany). After fixation in 4% paraformaldehyde, the slides were washed with PBS, quenched with glycine (100 mM glycine and 0.1% sodium azide in PBS), and blocked with PBS containing 2% BSA, 5% goat serum, and 0.2% Triton X-100 for 1 h at room temperature. Subsequently, tissues were incubated with the anti-Laminin antibody diluted at 1:1000 in the same blocking buffer overnight at 4°C and the DyLight® 594 conjugated goat anti-rabbit IgG (1:1000 dilution) for 1 h at room

Please cite this article as: D. Huang, F. Yue, J. Qiu et al., Polymeric nanoparticles functionalized with muscle-homing peptides for targeted delivery of phosphatase and tensin homolog inhibitor to skeletal muscle, Acta Biomaterialia, https://doi.org/10.1016/j.actbio.2020.10.009

temperature. Nuclei were counterstained with 4′,6-diamidino-2-phenylindole (DAPI, 1 μg/mL), which was premixed with the secondary antibody. Fluorescent images were captured using a CoolSnap HQ charge coupled-device camera equipped on a Leica DM 6000B microscope with a × 20 objective. Quantitative analysis of relative fluorescence intensity of AF488 in gastrocnemius sections and within myofibers was performed using ImageJ software. For each group, four animals were included with at least three images per animal analyzed.

2.9. Western blot analysis of PTEN downstream targets

C2C12 myoblasts were seeded onto 6-well plates at a density of 3×10^4 cells per well. After 24 h of culture, free VO-OHpic solution or VO-OHpic loaded PLGA-PEG-M12 NP suspension was added into the culture medium at a final VO-OHpic concentration of 10 μM and cells were further cultured for 12 or 24 h. The cells treated with DMSO vehicle only and blank PLGA-PEG-M12 NPs without encapsulating drugs were used as negative controls. Total protein was extracted from cells using RIPA buffer containing 25 mM Tris-HCl (pH 8.0), 150 mM NaCl, 1 mM EDTA, 0.5% NP-40, 0.5% sodium deoxycholate and 0.1% SDS. Protein concentrations were determined by Pierce BCA Protein Assay Reagent (Pierce Biotechnology, Waltham, MA, USA). Proteins were separated by SDS-PAGE and transferred to a polyvinylidene fluoride membrane (Millipore, Burlington, MA, USA). The membrane was then blocked with 5% fat-free milk for 1 h at room temperature and incubated with primary antibodies in 5% milk overnight at 4°C as well as secondary antibodies for 1 h at room temperature. Primary antibodies, including pAKT (1:2000 dilution), AKT (1:2000 dilution), pS6 (1:2000 dilution), S6 (1:2000 dilution), and β-Actin (1:5000 dilution), were used. HRP-conjugated secondary antibodies, including anti-rabbit and anti-mouse IgG, were also used at a dilution of 1:10,000. A luminol reagent for enhanced chemiluminescence detection of western blots (Santa Cruz Biotechnology, Dallas, TX, USA) was employed and signals were detected with a FluorChem R imaging system (ProteinSimple, San Jose, CA, USA).

2.10. Assessment of cell viability

In vitro cell viability after incubation with free VO-OHpic or VO-OHpic loaded PLGA-PEG-M12 NPs was determined using an MTS assay, which is based on the mitochondrial conversion of a tetrazolium salt. C2C12 cells were seeded onto 96-well plates at a density of 1×10^3 cells per well and cultured for 24 h. Blank NPs, VO-OHpic loaded NPs, or free VO-OHpic solutions were then added to the cells in culture medium at a final drug concentration of 10 μM and cells were further cultured for 12, 24, or 48 h. Subsequently, 20 μL of CellTiter 96® AQ_{ueous} one solution reagent was added to each well in 100 μL of culture medium and incubated at 37°C in a humidified, 5% CO_2 atmosphere for 2 h. The absorbance was measured using a Tecan Spark™ 10M microplate reader (Tecan, Männedorf, Switzerland) at a wavelength of 490 nm with background subtraction at 680 nm. Cells incubated with 0.1% Triton X-100 and DMSO vehicle only in culture medium served as positive and negative controls, respectively.

2.11. Statistical analysis

All studies were performed at least in triplicate and data points were expressed as mean values plus or minus standard error of the mean (mean ± SEM). To determine statistical significance, analysis of variance (one-way or two-way ANOVA) followed by Tukey's multiple comparison test was performed using GraphPad Prism 7. Differences were considered statistically significant if $p \leq 0.05$.

3. Results

3.1. NP preparation and characterization

The PTEN inhibitor VO-OHpic was encapsulated into PLGA-PEG NPs with or without M12 conjugation using the emulsion solvent evaporation technique with an encapsulation efficiency of 62.86%. A schematic morphological illustration of VO-OHpic encapsulated PLGA-PEG-M12 NPs is shown in Fig. 1A. The muscle-homing peptide M12 was covalently conjugated to PLGA-PEG NPs via the N-terminal α-amino groups of peptides using the N-hydroxysuccinimide ester reaction. M12 has previously shown high binding affinity to skeletal muscle and heart, homing antisense oligonucleotide-carrying cargos to local tissues following systemic administration [24]. The morphology of PLGA-PEG-M12 NPs encapsulating VO-OHpic was visualized using transmission electron microscopy. As shown in Fig. 1B, NPs appeared as dispersed spheres with a particle size of around 100 nm, exhibiting a dark core surrounded by a lighter gray rim corresponding to the hydrophilic PEG shell. The density of NPs after M12 conjugation became nonuniform, which was not seen in unconjugated NPs and probably related to the distribution of peptides on the surface of NPs. Results obtained by dynamic light scattering showed that PLGA-PEG-M12 NPs possessed an average particle size of 123.2 ± 1.3 nm and a relatively narrow size distribution with a polydispersity index of 0.067 ± 0.018 (Fig. 1C). The zeta potential was in the range of -23.9 ± 1.7 mV, preventing particle aggregation in suspension. To evaluate the release characteristics of VO-OHpic from NPs, we investigated *in vitro* release profiles of VO-OHpic encapsulated PLGA-PEG NPs and PLGA-PEG-M12 NPs under a neutral condition (phosphate-buffered saline, pH 7.4) at 37°C. Fig. 1D shows the cumulative amounts of VO-OHpic released from NPs as a function of time. The encapsulated NPs presented highly sustained release of VO-OHpic for as long as 16 days with over 50% of the encapsulated VO-OHpic released within the first three days. Also, the conjugation of M12 did not alter the release characteristics of VO-OHpic from PLGA-PEG NPs.

3.2. M12 mediates enhanced cellular uptake of NPs in myoblasts in vitro

To evaluate the active targeting of PLGA-PEG-M12 NPs to muscle cells, we examined *in vitro* cellular uptake of PLGA-PEG NPs and PLGA-PEG-M12 NPs in C2C12 myoblasts using fluorescence microscopy. C2C12 cells were incubated with PLGA-PEG NPs or PLGA-PEG-M12 NPs encapsulating a fluorescent dye Nile red to facilitate visualization. As shown in Fig. 2A, a well-dispersed red fluorescent signal originating from Nile red encapsulated PLGA-PEG NPs was detected within the cytoplasm and around the nucleus after 1 h of incubation, indicating that PLGA-PEG NPs have been rapidly taken up by C2C12 cells. The negative surface charge of NPs leads to repulsion between particles, thus preventing agglomeration and stabilizing NP dispersion inside the cells. When C2C12 cells were incubated with PLGA-PEG-M12 NPs, the intracellular red fluorescence intensity was remarkably enhanced compared to the PLGA-PEG NP treatment, suggesting that PLGA-PEG-M12 NPs were internalized by C2C12 cells to a greater extent than nontargeted NPs. Quantitative analysis showed a 2.44-fold increase in the cellular uptake efficiency of NPs after surface engineering with M12 (Fig. 2B, $p \leq 0.001$).

To further verify the specific interaction between PLGA-PEG-M12 NPs and surface receptors of C2C12 myoblasts, we performed competitive binding experiments by preincubating C2C12 cells with free M12 solution at a concentration of 50 μM to saturate its receptors present on the cell surface prior to treatment with PLGA-PEG-M12 NPs. Our results showed that the intracel-

Please cite this article as: D. Huang, F. Yue, J. Qiu et al., Polymeric nanoparticles functionalized with muscle-homing peptides for targeted delivery of phosphatase and tensin homolog inhibitor to skeletal muscle, Acta Biomaterialia, https://doi.org/10.1016/j.actbio.2020.10.009

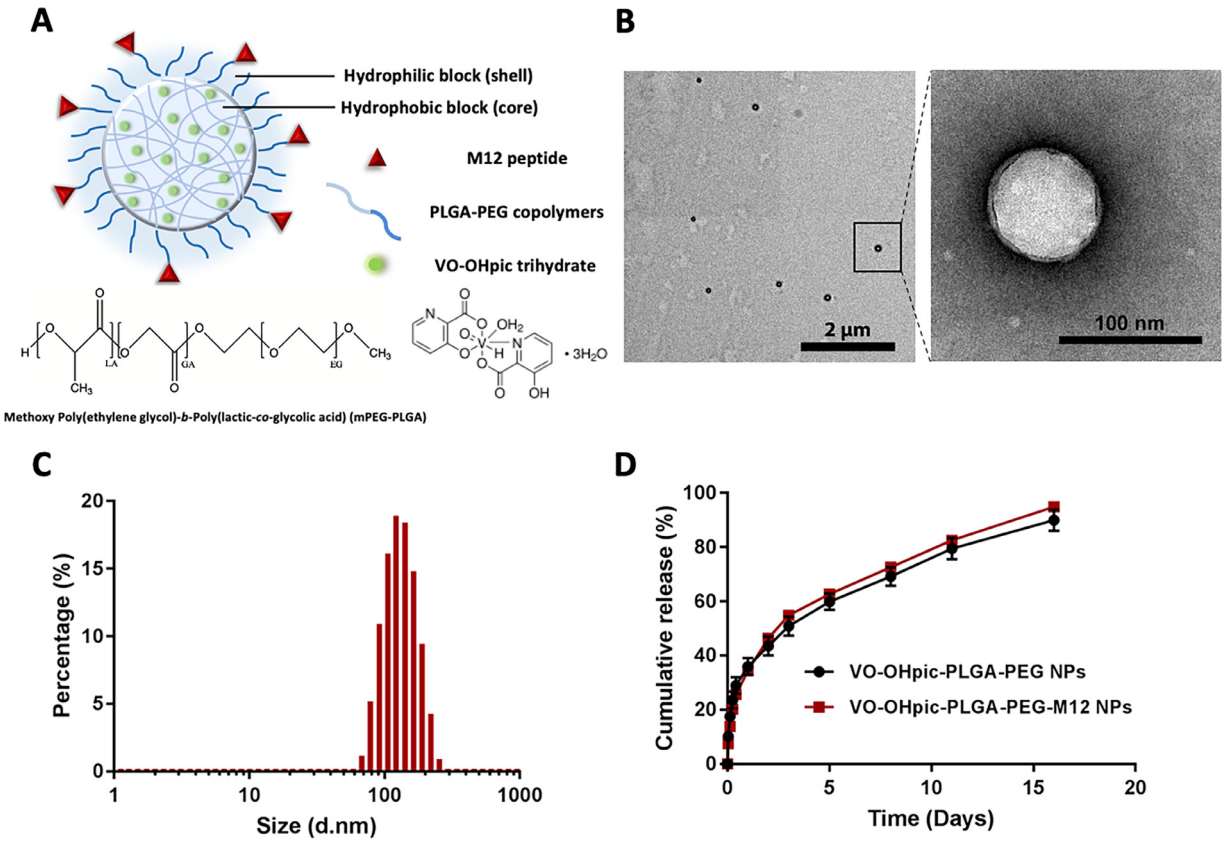

Fig. 1. NP preparation and characterization. (A) Schematic illustration of PLGA-PEG-M12 NPs encapsulating VO-OHpic trihydrate. The nanoparticulate delivery system consists of two components: (i) an outer PEG surface conjugated with a muscle-homing peptide M12, which can preferentially bind to the skeletal muscle, and (ii) a PLGA hydrophobic core that serves as a polymer matrix to encapsulate a PTEN inhibitor VO-OHpic trihydrate, promotes retention of the loaded drug inside the NP core, and controls drug release. Nontargeted and M12 functionalized NPs encapsulating VO-OHpic trihydrate were prepared using the single-step emulsion technique; (B) Representative transmission electron microscopy images of VO-OHpic loaded PLGA-PEG-M12 NPs; (C) Size distribution of VO-OHpic encapsulated PLGA-PEG-M12 NPs determined by dynamic light scattering; (D) *In vitro* release profiles of VO-OHpic from PLGA-PEG NPs and PLGA-PEG-M12 NPs.

lular red fluorescence intensity after free M12 pretreatment significantly decreased compared to incubation with PLGA-PEG-M12 NPs alone ($p \leq 0.001$), indicating that the interaction between PLGA-PEG-M12 NPs and receptors in C2C12 cells as well as the subsequent M12 receptor-mediated endocytosis were suppressed due to ligand competition with free M12. In contrast, preincubation with M12 did not affect cellular internalization of PLGA-PEG NPs ($p > 0.05$). We also investigated the cellular uptake of NPs in 3T3-L1 preadipocytes to confirm the specificity of M12 receptors in muscle cells. As shown in Fig. 2A and C, neither enhanced cellular uptake nor binding inhibition was observed in 3T3-L1 cells. These data support that M12 mediates more efficient cellular uptake of NPs in myoblasts *in vitro* compared to non-specific internalization.

In addition to the targeting capacity of M12 to murine C2C12 myoblasts and myofibers, our preliminary validation data have also shown that M12 exhibited high binding affinity to human skeletal myoblasts (Supplementary Fig. S1), suggesting the target epitope might also be present in human muscles. To investigate whether PLGA-PEG-M12 NPs could achieve active targeting to human cells, we subsequently examined *in vitro* cellular uptake of PLGA-PEG NPs and PLGA-PEG-M12 NPs in human skeletal myoblasts. Similar to the results observed in the C2C12 experiments, a well-dispersed red fluorescent signal arising from Nile red encapsulated NPs was detected in the cytoplasm in both treatment groups, indicating quick cellular uptake of NPs in human skeletal myoblasts (Fig. 2D). Compared to PLGA-PEG NPs, the incubation of PLGA-PEG-M12 NPs resulted in a significant increase in cellular internalization, suggesting M12 mediates enhanced NP delivery to human muscle cells (Fig. 2E, $p \leq 0.001$).

3.3. *M12 facilitates active targeting of NPs to skeletal muscle following systemic administration* in vivo

To assess the targeting efficiency of PLGA-PEG-M12 NPs to skeletal muscle *in vivo*, we examined the biodistribution of Alexa Fluor® 488 conjugated NPs (AF488-PLGA-PEG NPs and AF488-PLGA-PEG-M12 NPs) in *mdx* mice following intravenous injection using a fluorescence optical imaging system. The fluorescent dye AF488-NHS ester was conjugated to PLGA-PEG-NH_2 through amide bond formation followed by NP preparation using the standard protocol. The experimental design representing the timeline of NP injection is shown in Fig. 3A. AF488-PLGA-PEG NPs or AF488-PLGA-PEG-M12 NPs in saline at a concentration of 80 mg/kg were injected into the tail vein of *mdx* mice. After 6 h of administration, AF488-PLGA-PEG-M12 NPs presented an intense fluorescence signal in the whole hindlimbs, whereas only minimal accumulation of nontargeted NPs (AF488-PLGA-PEG NPs) was detected in the hindlimb muscle tissue (Fig. 3B).

After whole-body imaging, mice were immediately euthanized and various tissues, including the liver, kidney, spleen, heart, and skeletal muscle, were dissected for *ex vivo* imaging. As shown in Fig. 3C, results revealed that the fluorescence signal arising from AF488-PLGA-PEG-M12 NPs was exclusively detected in the heart and skeletal muscle, including quadriceps, gastrocnemius, and diaphragm, although there was nonspecific accumulation in the liver

Please cite this article as: D. Huang, F. Yue, J. Qiu et al., Polymeric nanoparticles functionalized with muscle-homing peptides for targeted delivery of phosphatase and tensin homolog inhibitor to skeletal muscle, Acta Biomaterialia, https://doi.org/10.1016/j.actbio.2020.10.009

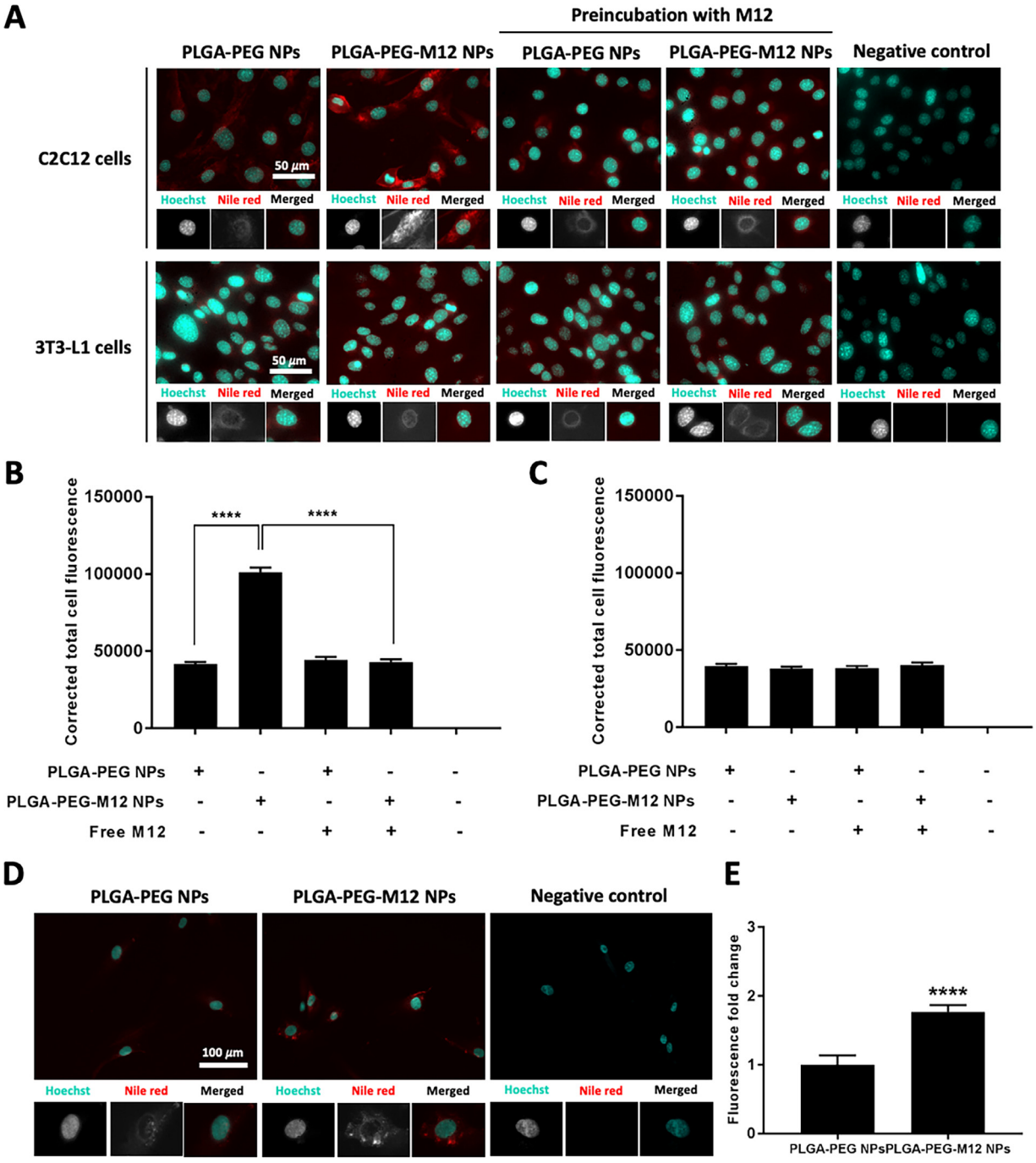

Fig. 2. M12 mediates enhanced cellular uptake of NPs in myoblasts *in vitro*. (A) Representative fluorescence microscopy images of C2C12 myoblasts and 3T3-L1 preadipocytes treated with Nile red encapsulated PLGA-PEG NPs or PLGA-PEG-M12 NPs for 1 h with or without preincubation of free M12 solution. The final NP concentration was 0.1 mg/mL and free M12 at a concentration of 50 μM was used to saturate the specific binding receptors of M12 on the cell surface. A negative control without any NP treatment was also included; (B) Quantitative analysis of corrected total cell fluorescence intensity indicating cellular uptake of Nile red encapsulated NPs in C2C12 myoblasts. 200-300 cells in total from three individual repeats were analyzed for each group; (C) Quantitative analysis of corrected total cell fluorescence intensity indicating cellular uptake of Nile red encapsulated NPs in 3T3-L1 preadipocytes; (D) Representative fluorescence microscopy images of human skeletal myoblasts treated with Nile red encapsulated PLGA-PEG NPs or PLGA-PEG-M12 NPs at a concentration of 0.1 mg/mL for 1 h; (E) Quantitative analysis of fluorescence intensity indicating cellular uptake of Nile red encapsulated NPs in human skeletal myoblasts. (For interpretation of the references to color in this figure legend, the reader is referred to the web version of this article.).

and kidney due to active metabolism. The injection of nontargeted AF488-PLGA-PEG NPs led to a relatively homogeneous distribution of NPs in all the organs or tissues throughout the body with significantly reduced fluorescence signals in skeletal muscle compared to those in the targeted AF488-PLGA-PEG-M12 NP group. These results were consistent with the findings from the whole-body imaging, indicating the muscle-homing property of M12. Based on the biodistribution results, the fluorescence intensity of skeletal muscle was quantified for each individual muscle group and normalized to that of the liver, which is the main metabolic detoxification organ of the body. Compared to nontargeted NPs, 1.23, 1.69, 2.31, and 1.91-fold increases in the fluorescence ratio were observed in the heart, quadriceps, gastrocnemius, and diaphragm, respectively in the mice injected with AF488-PLGA-PEG-M12 NPs (Fig. 3D). The difference in gastrocnemius muscle between two groups was statistically significant ($p \leq 0.05$). The data reveal that the conjugation

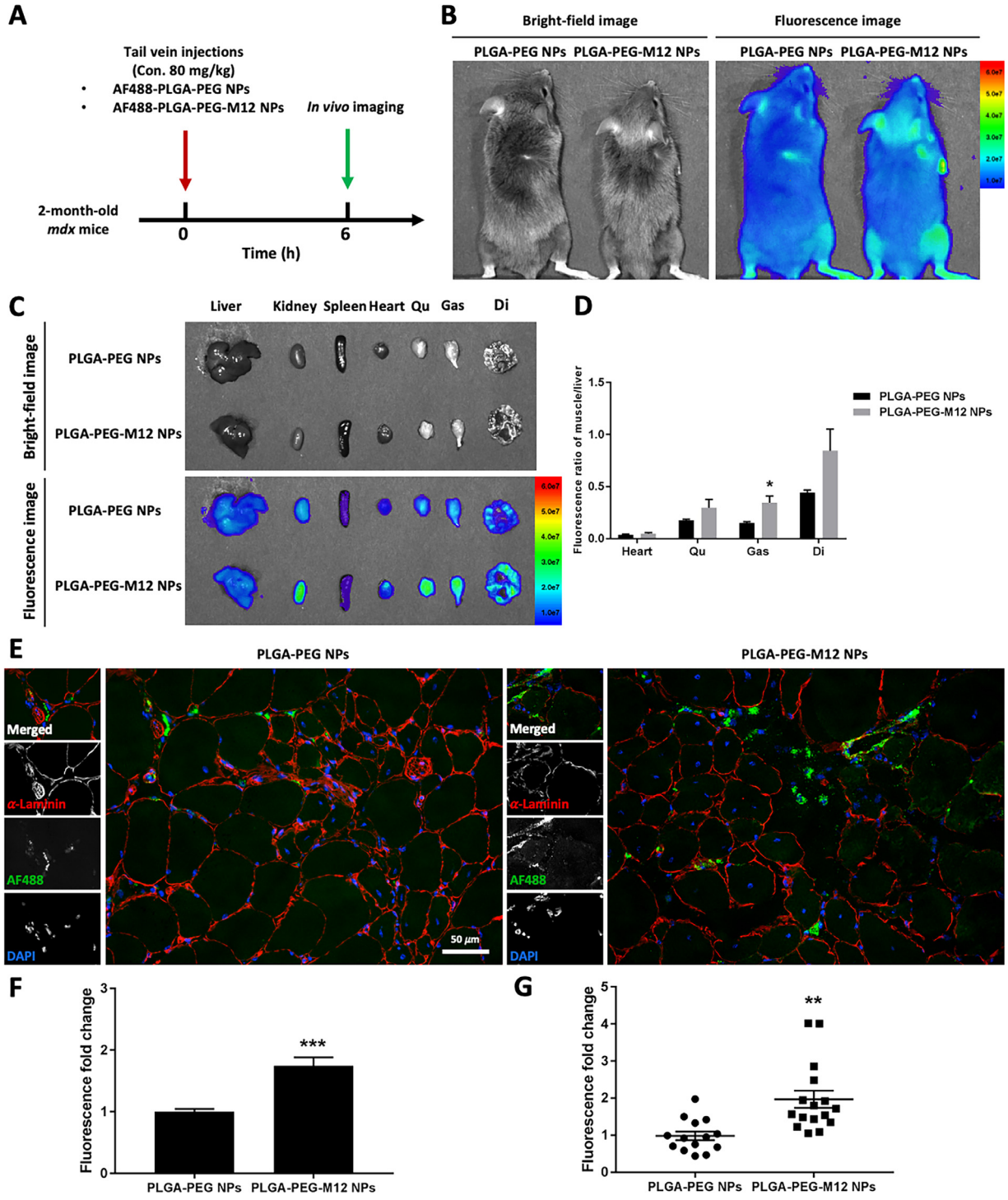

Fig. 3. M12 facilitates active targeting of NPs to skeletal muscle following systemic administration *in vivo*. (A) Experimental design showing the timeline of NP injection in dystrophin-deficient *mdx* mice; (B) Whole-body imaging of fluorescent AF488 dye conjugated NPs (AF488-PLGA-PEG NPs or AF488-PLGA-PEG-M12 NPs) in the hindlimbs of mice at 6 h post intravenous injection; (C) Biodistribution of fluorescent AF488 dye conjugated NPs in different dissected tissues, including the liver, kidney, spleen, heart, quadriceps (Qu), gastrocnemius (Gas), and diaphragm (Di); (D) Quantitative analysis of fluorescence ratio of muscle to liver. The fluorescence intensity of each tissue was measured by the optical imaging system and calculated based on the default equation from the system. The fluorescence ratio of muscle to liver was obtained by dividing the fluorescence intensity of liver with that of each muscle tissue, respectively (n = 4); (E) Representative images of 10 μm-thick gastrocnemius sections stained with α-Laminin antibody and DAPI and observed under a fluorescence microscope at 200 × magnification; (F) Quantitative analysis of relative fluorescence intensity of AF488 in gastrocnemius sections. For each group, four animals were included with at least three images per animal analyzed; (G) Quantitative analysis of relative fluorescence intensity of AF488 within myofibers. At least 12 images were analyzed from four animals in each group with each dot representing one image.

Please cite this article as: D. Huang, F. Yue, J. Qiu et al., Polymeric nanoparticles functionalized with muscle-homing peptides for targeted delivery of phosphatase and tensin homolog inhibitor to skeletal muscle, Acta Biomaterialia, https://doi.org/10.1016/j.actbio.2020.10.009

of M12 achieves a selective enhancement in total NP localization in muscle tissues with minimizing the undesired accumulation in off-target organs.

We subsequently sectioned the gastrocnemius muscle to further determine the distribution of NPs within the tissue. As shown in Fig. 3E, green fluorescence signals arising from NPs were detected only in limited regions in muscle sections of AF488-PLGA-PEG NP treated mice. The intensity and area of fluorescence signals substantially increased in the section collected from the mice injected with AF488-PLGA-PEG-M12 NPs compared to those in the AF488-PLGA-PEG NP group, demonstrating M12-mediated NP accumulation in the gastrocnemius muscle. Quantitative analysis further confirmed a 1.7-fold increase in the intensity of total AF488 fluorescence in muscle sections in the M12 conjugated NP group compared to that acquired in the nontargeted NP group (Fig. 3F, $p \leq 0.005$). Interestingly, it was observed that a portion of AF488-PLGA-PEG-M12 NPs were localized inside myofibers within the time intervals analyzed, whereas fluorescence signals were barely seen within myofibers in the AF488-PLGA-PEG NP group (Fig. 3E). Quantification results showed that the intensity of AF488 fluorescence within myofibers in the AF488-PLGA-PEG-M12 NP group was approximately 2.1-fold higher than that in the AF488-PLGA-PEG NP group (Fig. 3G, $p \leq 0.01$), suggesting that M12 might facilitate the binding of NPs to myofibers and subsequent permeation across the myofiber membrane. Nevertheless, the basal lamina and myofiber sarcolemma posed a significant delivery barrier for NPs as the majority of fluorescent NPs were retained in the extracellular matrix in both formation groups at the time point examined (i.e. 6 h post injection).

3.4. *Encapsulation of VO-OHpic into PLGA-PEG-M12 NPs achieves sustained inhibition of PTEN signaling without causing cytotoxicity* in vitro

The effects of VO-OHpic on the PTEN signaling, including protein levels of PTEN, AKT, and ribosomal S6 kinase, were determined by western blot analysis. AKT and ribosomal S6 kinase are downstream targets in the PTEN signaling pathway with inhibition of PTEN signaling leading to activation of phosphorylated AKT and ribosomal S6 kinase [27]. Our results showed that the treatment with VO-OHpic free drug or VO-OHpic encapsulated PLGA-PEG-M12 NPs at a concentration of 10 μM did not cause any significant changes in the protein level of PTEN (Supplementary Figure S2), while significantly upregulated the protein expression of pAKT ($p \leq 0.005$) and pS6 ($p \leq 0.001$), suggesting efficient inhibition of enzymatic activity of PTEN (Fig. 4A–C). However, we were unable to evaluate for a longer time point due to the limitation in cell viability. The expression levels of pAKT and pS6 were consistently increased when cells were incubated with VO-OHpic loaded PLGA-PEG-M12 NPs for 12 h. It was noticed that the upregulation in pAKT expression induced by VO-OHpic loaded NPs ($p \leq 0.001$) was even more significant than that in the free drug group, which might be attributed to enhanced intracellular delivery of NPs to myoblasts. When the incubation time of NPs was extended to 24 h, the protein levels of pAKT ($p \leq 0.05$) and pS6 ($p \leq 0.001$) maintained constantly upregulated, indicating efficient and sustained inhibition of PTEN signaling achieved by VO-OHpic loaded NPs.

The cytotoxicity of VO-OHpic free drug and VO-OHpic loaded PLGA-PEG-M12 NPs in C2C12 myoblasts was also determined using an MTS assay. C2C12 cells were incubated with VO-OHpic free drug or VO-OHpic loaded NPs for 12, 24, and 48 h and results were normalized to the vehicle control groups. It was found that free VO-OHpic at the concentration used resulted in a decline in cell viability in a time-dependent manner (Fig. 4D). Although the treatment did not cause detectable cytotoxicity within the first 12 h, the cell viability significantly decreased to 64.78% ($p \leq 0.05$) and 45.73% ($p \leq 0.01$) after 24 h and 48 h of incubation, respectively. In contrast, the cell viability was well maintained after the treatment with VO-OHpic loaded NPs at comparable drug concentrations throughout the entire culture period, indicating that encapsulation of VO-OHpic into PLGA-PEG-M12 NPs exhibited a great improvement in the safety of PTEN inhibitor and preserving the viability of muscle cells. Also, no obvious cytotoxicity was observed in the group treated with blank NPs, suggesting the superior biocompatibility of M12 conjugated NP delivery system. These results together provide encouraging evidence that encapsulation of VO-OHpic into PLGA-PEG-M12 NPs achieves efficient inhibition of PTEN signaling without causing cytotoxicity.

4. Discussion

At present, most clinical practices for the treatment of DMD are palliative at best, aimed at managing issues with ambulation, respiratory function, and cardiac health that are typical of DMD [28]. In addition to conventional therapeutic strategies, a number of advanced approaches have been explored to date with varying degrees of success. For instance, cell-based therapy is used to reconstitute the satellite cell pool with dystrophin competent cells, thereby restoring muscle function. Multiple cell types have been applied in transplantation experiments in DMD animal models or patents, including myoblasts, bone marrow cells, and pluripotent stem cells [29]. Gene therapy, such as antisense oligoribonucleotide-mediated exon skipping, has also shown much promise and has spurred the investigation of numerous pharmaceuticals, one of which is eteplirsen, the first and currently only FDA-approved drug for the treatment of DMD [30]. These therapeutic options for DMD represent the first step toward the development of curative therapies for this devastating disorder. However, several challenges, including improvement of delivery systems, distribution to all diseased tissues, achievement of a sustainable therapeutic efficacy for life-long treatment still remain to be overcome.

Consequently, alternative approaches aimed at regulating skeletal muscle signaling pathways have been proposed for DMD treatment. We have recently discovered the critical role of PTEN signaling in the pathogenesis of DMD. It has been demonstrated that pharmacological inhibition of PTEN signaling through three weeks of consecutive daily dosing of a PTEN inhibitor VO-OHpic trihydrate substantially reduces the dystrophic symptoms. Specifically, the beneficial phenotypes of PTEN inhibition result in improved muscular strength and prolonged ambulation. However, a relatively high dose of drug is required to modulate skeletal muscle function in all affected tissues when using conventional delivery approaches, which might in turn cause off-target drug accumulation in other organs and potential side effects. Site-specific and controlled delivery of the PTEN inhibitor to massively expanded skeletal muscle using NPs could minimize off-target adverse effects and maximize the therapeutic efficacy of the drug. Targeted NPs have shown tremendous therapeutic potential in both research and clinical settings and are widely expected to lead to rapid changes in the landscape of pharmaceutical industry [20]. Here, we use the M12 peptide to facilitate NP homing to skeletal muscle specifically. A recent study has employed a phage display library on C2C12 myoblasts to identify that M12 preferentially binds to skeletal muscle after systemic administration in adult *mdx* mice [24]. When M12 is conjugated to phosphorodiamidate morpholino oligomer, the conjugates effectively induce exon skipping and dystrophin restoration in skeletal muscle [24–26]. By conjugating this short muscle-homing peptide to polymeric NPs, we developed a robust drug delivery platform that carries a hydrophobic PTEN inhibitor and investigated their muscle-targeting specificity and inhibitory effects on the PTEN signaling as a proof of concept.

Please cite this article as: D. Huang, F. Yue, J. Qiu et al., Polymeric nanoparticles functionalized with muscle-homing peptides for targeted delivery of phosphatase and tensin homolog inhibitor to skeletal muscle, Acta Biomaterialia, https://doi.org/10.1016/j.actbio.2020.10.009

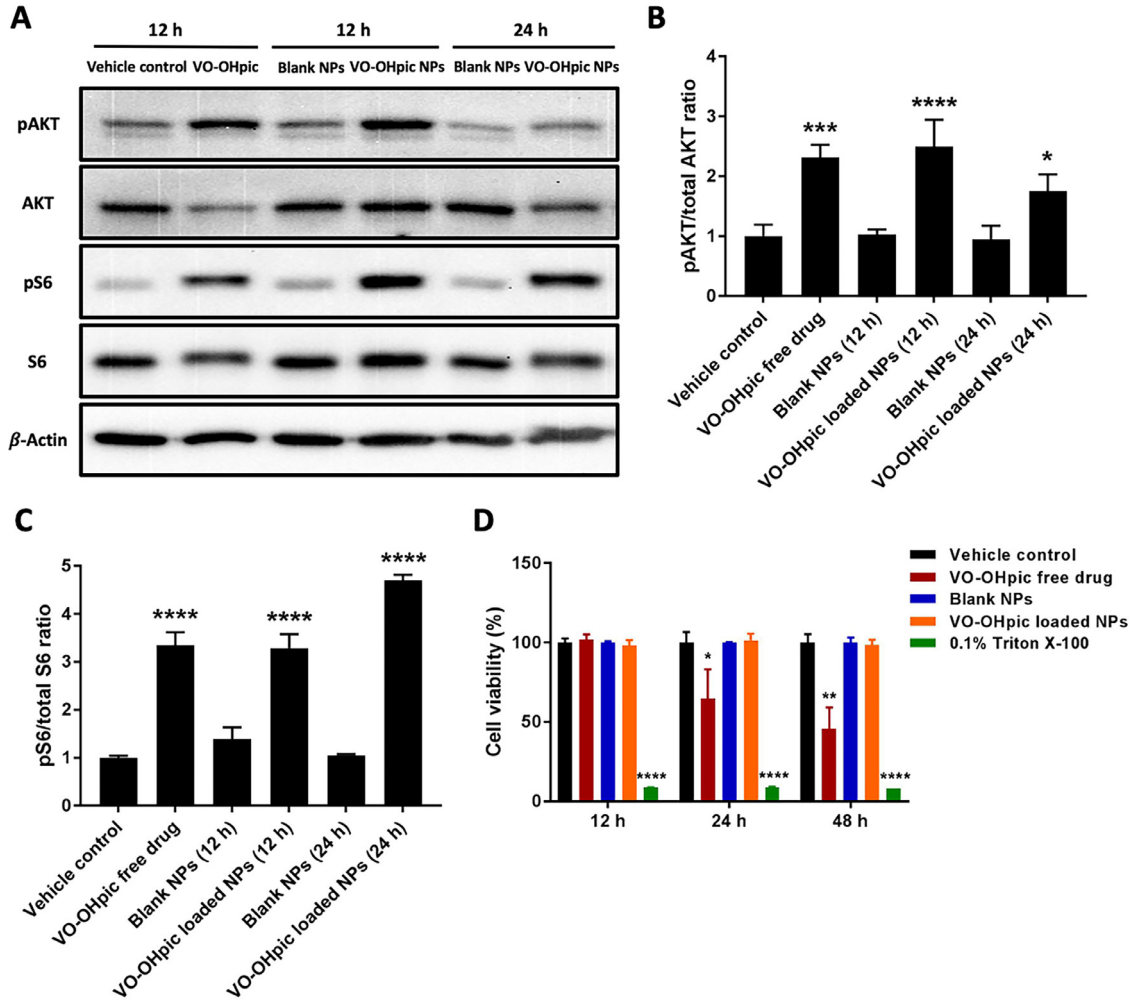

Fig. 4. Encapsulation of VO-OHpic into PLGA-PEG-M12 NPs achieves sustained inhibition of PTEN signaling without causing cytotoxicity *in vitro*. (A) Western blot analysis of pAKT and pS6 protein expression in C2C12 myoblasts after treatment with VO-OHpic free drug and VO-OHpic loaded PLGA-PEG-M12 NPs. Cells were incubated with free VO-OHpic solution or VO-OHpic loaded NP suspension in culture medium with a final VO-OHpic concentration of 10 μM for 12 or 24 h. Cells in the vehicle control group were treated with DMSO vehicle only and the blank NP group received the treatment of blank PLGA-PEG-M12 NPs without encapsulating the drug; (B) Quantification of protein expression levels of pAKT normalized to total AKT controls by densitometry analysis (n =3); (C) Quantification of protein expression levels of pS6 normalized to total S6 controls by densitometry analysis (n =3); (D) Cell viability of C2C12 myoblasts after treatment with VO-OHpic free drug, blank PLGA-PEG-M12 NPs, and VO-OHpic loaded PLGA-PEG-M12 NPs for different periods of time (12, 24, and 48 h) as determined by MTS assay. Cells incubated with 0.1% Triton X-100 and DMSO vehicle only in culture medium served as positive and negative controls, respectively (n =3).

PLGA-PEG-M12 NPs formulated in this study exhibit unique physicochemical properties, including small particle size, narrow size distribution, and highly negative surface charge. All these characteristics are considered to favor efficient drug delivery to the target cells and tissues. Furthermore, the loading amount of VO-OHpic within PLGA-PEG-M12 NPs was found to be 9.43 μg per mg of NPs, which is sufficient to elicit therapeutic effects for PTEN inhibition when released properly. The encapsulated VO-OHpic appeared to be released over a period of approximately two weeks in a biphasic manner, characterized by an initial rapid release phase followed by more sustained release. A significant initial burst was observed with 34.42% of the encapsulated drug released from NPs within the first day, which might be due to the VO-OHpic molecules that loosely bound or inserted among PEG chains on the surface of NPs [31]. After the initial burst, VO-OHpic release profiles displayed a sustained fashion. This slow release could result from the diffusion of VO-OHpic into polymer matrix and the drug molecules through polymer wall as well as the erosion of polymers. The drug molecules attached to the NP surface may migrate into the interior matrix during the formulation process with the carrier matrix maintaining a compact interconnected network structure to restrain drug release.

The present cellular uptake studies highlight the potential of PLGA-PEG-M12 NPs for targeted drug delivery to muscle cells. The specific binding between particulate drug carriers and specific cells that leads to selective cellular uptake is of particular importance for targeted delivery of therapeutics, especially to the intracellular space [32,33]. In our studies, targeted NP internalization in C2C12 and human skeletal myoblasts was achieved by modifying the surface of NPs with M12, which has been confirmed to preferentially bind to biologically active molecules or receptors present on the surface of muscle cells [24]. Achievement of active targeting of NPs to myoblasts and subsequent drug release within the cells would be beneficial for the treatment of DMD. A previous study has demonstrated that dystrophin is expressed in activated satellite cells, where it regulates the establishment of satellite cell polarity and asymmetric cell division. Their findings indicate that dysfunctions in dystrophin-deficient myoblasts also contribute to muscle wasting and disease progression of DMD. Therefore, therapies targeting myoblasts could hold great potential for the treatment of DMD [34]. Although M12 has exhibited unique properties

Please cite this article as: D. Huang, F. Yue, J. Qiu et al., Polymeric nanoparticles functionalized with muscle-homing peptides for targeted delivery of phosphatase and tensin homolog inhibitor to skeletal muscle, Acta Biomaterialia, https://doi.org/10.1016/j.actbio.2020.10.009

for serving as an actively targeted ligand to enhance the specificity and efficiency of NP-mediated drug delivery to skeletal muscle, a major limitation is that the potential binding receptor of M12 still remains unclear. The amino acid sequence of M12 does not match any known motif by searching across several databases, including SAROTUP, PEPBANK, nonredundant protein sequences, Swiss-Prot, patented protein sequences, and Protein Data Bank [24]. Also, no conserved motif is present in the sequence composition of M12 and other muscle-specific peptides except serine [35,36]. Further investigation in determining the potential binding receptor of M12 and the relationship between structure and ligand-receptor interaction would throw light on how the peptide ligand mediates cellular uptake of NPs in different cell types. Nevertheless, this is the first study demonstrating the concept that muscle-homing peptides are able to facilitate enhanced intracellular delivery of NPs to skeletal muscle.

Our *in vivo* results further confirm that PLGA-PEG-M12 NPs efficiently target skeletal muscle tissues following intravenous administration. An increased proportion of PLGA-PEG-M12 NPs were found to rapidly distribute in muscle tissues compared to nontargeted NPs, although there was nonspecific accumulation in the liver and kidney. The observed biodistribution of NPs is related to the fact that a predominant portion of systemically injected NPs face either sequestration by the liver or filtration by the kidney [37]. It was also noted that the fluorescence intensity in the liver was comparable between the two groups; however, a higher amount of PLGA-PEG-M12 NPs were accumulated in the kidney than PLGA-PEG NPs. The detected difference was in agreement with the observation in the biodistribution of free M12 peptides demonstrating that the conjugation of hydrophilic M12 might affect the physicochemical characteristics of NPs, thereby leading to slightly different dynamic profiles of NPs via the systemic circulation. Interestingly, we found that a portion of PLGA-PEG-M12 NPs have penetrated across the membrane and localized within myofibers, which was barely seen in the nontargeted PLGA-PEG NP group. The close proximity of NPs to the target site would greatly improve delivery efficiency of the encapsulated drug and subsequent therapeutic consequences. This is particularly beneficial for hydrophobic drugs, such as VO-OHpic, which in general are delivered less effectively than water-soluble compounds in native forms. After being localized in the target tissue, the released drug would be better retained *in situ* to sustain its therapeutic action with a constantly efficient concentration over a prolonged period of time. Dystrophic muscle typically displays an accelerated rate of turnover with active cycles of myofiber degeneration and regeneration compared to normal muscle, which might have an impact on the drug clearance in skeletal muscle [38]. The use of NPs coupled with a PTEN inhibitor that reduces the rate of myofiber turnover might effectively minimize the required frequency of readministration and maximize the therapeutic efficacy.

Although M12 conjugated NPs showed enhanced and muscle-specific accumulation after systemic delivery, the majority of NPs were retained in the extracellular matrix with limited internalization/penetration into myofibers at the time point examined (i.e. 6 h post injection). This might be due to the relatively short time interval between injection and tissue analysis and the low preservation of NPs within myofibers during muscle cryosection. In addition, the extracellular matrix (endomysium) and sarcolemma of myofiber may represent a significant barrier for NPs to penetrate. This challenge could be overcome by further optimization of our delivery system (e.g. combining M12 with other membrane penetrating ligands or transiently increasing the membrane permeability). It is also worth noting that myofibers are not the only therapeutic target for the treatment of DMD. Alternatively, targeting muscle stem cells, including satellite cells and myoblasts, is equally important and may be more advantageous. Myoblast-based cell and gene therapy has been widely investigated to treat muscular dystrophy due to their key roles in muscle regeneration [34]. For therapeutic intervention by PTEN inhibition, in particular, targeting myoblasts would provide enhanced therapeutic efficacy compared to targeting myofibers, as PTEN is expressed at much higher levels in muscle progenitor cells than in myofibers [39]. In our recent study, we also found that deletion of *Pten* in embryonic myoblasts ameliorates muscle wasting and improves muscle function in a mouse model of DMD [14]. Furthermore, even NPs are localized to the extracellular matrix without completely incorporating into myofibers, the released PTEN inhibitor at the periphery of dystrophic myofibers would also facilitate its diffusion and internalization into myofibers.

Lastly, we demonstrate that PLGA-PEG-M12 NPs encapsulating VO-OHpic achieve sustained PTEN inhibition with preservation of cell viability. Severe cytotoxicity in a time-dependent manner was induced by free VO-OHpic in myoblasts, as indicated by the cell viability data. One possible explanation for the observed cytotoxicity could be the acute inhibition of PTEN signaling, thus the overdose of PTEN inhibitor may result in a reduction in cell viability [40]. Also, vanadium compounds have been found to interact with mitochondria to enhance the respiratory metabolism and induce intracellular reactive oxygen species, which present cytotoxicity [41]. In contrast to free VO-OHpic, VO-OHpic encapsulated PLGA-PEG-M12 NPs maintained superior cell viability throughout the entire culture period. The use of nanoparticulate delivery system substantially improves the safety of vanadium complex by avoiding acute PTEN inhibition. Moreover, the slowly released VO-OHpic from NPs inside of myoblasts even in a small amount was sufficient to achieve effective inhibition of PTEN signaling. PTEN inhibition is known to modulate the intracellular AKT and ribosomal S6 kinase pathways, which are important for the control of skeletal muscle growth and hypertrophy [42]. Previous research has shown that activation of AKT expression and phosphorylation by overexpressing microRNA-486 improves muscular dystrophy-associated symptoms [43]. In our present study, VO-OHpic released from NPs effectively stimulated the activity of AKT and ribosomal S6 kinase. Unfortunately, we were not able to evaluate the long-term inhibitory effect of NPs due to the limitation in cell culture (i.e. C2C12 is a fairly quickly growing cell line with a short doubling time of approximately 12 h). However, with enhanced cellular internalization by targeted muscle cells and controlled drug release within the cells, sustained inhibition of PTEN signaling induced by M12 modified NPs can be expected under *in vivo* conditions.

5. Conclusions

We provide evidence of the validity of a muscle-targeted nanoparticulate drug delivery system. The results show, to our knowledge for the first time, polymeric NPs functionalized with a muscle-homing peptide greatly increase the cellular uptake efficiency of NPs in cultured myoblasts and their selective localization in skeletal muscle tissue (e.g. myofibers), potentially allowing enhanced therapeutic efficacy and minimizing off-target side effects. Moreover, the slowly released PTEN inhibitor from NPs reduces its cytotoxicity and achieves sustained inhibition of PTEN signaling, which would considerably improve long-term treatment outcomes. Although further optimization of NPs is required to improve their *in vivo* targeting efficiency particularly the penetration capability across the extracellular matrix, our design rationale has produced promising results through taking advantages of polymeric nanomaterials and muscle-homing peptides. This technique could potentially open a new avenue for the development of long-term therapeutic strategies in DMD treatment.

Please cite this article as: D. Huang, F. Yue, J. Qiu et al., Polymeric nanoparticles functionalized with muscle-homing peptides for targeted delivery of phosphatase and tensin homolog inhibitor to skeletal muscle, Acta Biomaterialia, https://doi.org/10.1016/j.actbio.2020.10.009

Declaration of Competing Interest

The authors declare that they have no conflict of interest with the contents of this article.

Acknowledgments

The authors appreciate the funding support from the Muscular Dystrophy Association (MDA516161 to F.Y.) and National Institute of Arthritis and Musculoskeletal and Skin Diseases (R01AR071649 to S. K.).

Supplementary materials

Supplementary material associated with this article can be found, in the online version, at doi:10.1016/j.actbio.2020.10.009.

References

[1] R.J. Fairclough, M.J. Wood, K.E. Davies, Therapy for Duchenne muscular dystrophy: renewed optimism from genetic approaches, Nat. Rev. Genet. 14 (2013) 373–378.
[2] J.M. Ervasti, K.P. Campbell, A role for the dystrophin-glycoprotein complex as a transmembrane linker between laminin and actin, J. Cell Biol. 122 (1993) 809–823.
[3] J.M. Ervasti, K.P. Campbell, Membrane organization of the dystrophin-glycoprotein complex, Cell 66 (1991) 1121–1131.
[4] E.P. Hoffman, R.H. Brown, L.M. Kunkel, Dystrophin: the protein product of the Duchene muscular dystrophy locus. 1987, Biotechnology 24 (1992) 457–466.
[5] K.P. Campbell, S.D. Kahl, Association of dystrophin and an integral membrane glycoprotein, Nature 338 (1989) 259–262.
[6] S. Dahiya, S. Bhatnagar, S.M. Hindi, C. Jiang, P.K. Paul, S. Kuang, A. Kumar, Elevated levels of active matrix metalloproteinase-9 cause hypertrophy in skeletal muscle of normal and dystrophin-deficient mdx mice, Hum. Mol. Genet. 20 (2011) 4345–4359.
[7] E.R. Barton, L. Morris, A. Musaro, N. Rosenthal, H. Lee Sweeney, Muscle-specific expression of insulin-like growth factor I counters muscle decline in mdx mice, J. Cell Biol. 157 (2002) 137–147.
[8] S.M. Gehrig, J.G. Ryall, J.D. Schertzer, G.S. Lynch, Insulin-like growth factor-I analogue protects muscles of dystrophic mdx mice from contraction-mediated damage, Exp. Physiol. 93 (2008) 1190–1198.
[9] P.P. Nghiem, J.N. Kornegay, K. Uaesoontrachoon, L. Bello, Y. Yin, A. Kesari, P. Mittal, S.J. Schatzberg, G.M. Many, N.H. Lee, E.P. Hoffman, Osteopontin is linked with AKT, FoxO1, and myostatin in skeletal muscle cells, Muscle Nerve 56 (2017) 1119–1127.
[10] K.R. Wagner, A.C. McPherron, N. Winik, S.J. Lee, Loss of myostatin attenuates severity of muscular dystrophy in mdx mice, Ann. Neurol. 52 (2002) 832–836.
[11] T. Maehama, J.E. Dixon, The tumor suppressor, PTEN/MMAC1, dephosphorylates the lipid second messenger, phosphatidylinositol 3,4,5-trisphosphate, J. Biol. Chem. 273 (1998) 13375–13378.
[12] J.N. Haslett, D. Sanoudou, A.T. Kho, R.R. Bennett, S.A. Greenberg, I.S. Kohane, A.H. Beggs, L.M. Kunkel, Gene expression comparison of biopsies from Duchenne muscular dystrophy (DMD) and normal skeletal muscle, Proc. Natl. Acad. Sci. U. S. A. 99 (2002) 15000–15005.
[13] M. Feron, L. Guevel, K. Rouger, L. Dubreil, M.C. Arnaud, M. Ledevin, L.A. Megeney, Y. Cherel, V. Sakanyan, PTEN contributes to profound PI3K/Akt signaling pathway deregulation in dystrophin-deficient dog muscle, Am. J. Pathol. 174 (2009) 1459–1470.
[14] F. Yue, C. Song, D. Huang, N. Narayanan, J. Qiu, Z. Jia, Z. Yuan, S.N. Oprescu, B.T. Roseguini, M. Deng, S. Kuang, PTEN inhibition ameliorates muscle degeneration and improves muscle function in a mouse model of Duchenne muscular dystrophy, BioRxiv (2020) 2020.08.13.249961.
[15] A.K. Srivastava, J.-L. Chiasson, Vanadium Compounds: Biochemical and Therapeutic Applications, Springer Science & Business Media, 1996.
[16] M.S. Kim, A. El-Fiqi, J.W. Kim, H.S. Ahn, H. Kim, Y.J. Son, H.W. Kim, J.K. Hyun, Nanotherapeutics of PTEN inhibitor with mesoporous silica nanocarrier effective for axonal outgrowth of adult neurons, ACS Appl. Mater. Interfaces 8 (2016) 18741–18753.
[17] R. Langer, Drug delivery and targeting, Nature (1998) 5–10.
[18] F. Alexis, E. Pridgen, L.K. Molnar, O.C. Farokhzad, Factors affecting the clearance and biodistribution of polymeric nanoparticles, Mol. Pharm. 5 (2008) 505–515.
[19] Y.R. Gokarn, M. McLean, T.M. Laue, Effect of PEGylation on protein hydrodynamics, Mol. Pharm. 9 (2012) 762–773.
[20] N. Kamaly, Z. Xiao, P.M. Valencia, A.F. Radovic-Moreno, O.C. Farokhzad, Targeted polymeric therapeutic nanoparticles: Design, development and clinical translation, Chem. Soc. Rev. 41 (2012) 2971–3010.
[21] N. Bertrand, J. Wu, X. Xu, N. Kamaly, O.C. Farokhzad, Cancer nanotechnology: the impact of passive and active targeting in the era of modern cancer biology, Adv. Drug Deliv. Rev. 66 (2014) 2–25.
[22] J.E. Zuckerman, I. Gritli, A. Tolcher, J.D. Heidel, D. Lim, R. Morgan, B. Chmielowski, A. Ribas, M.E. Davis, Y. Yen, Correlating animal and human phase Ia/Ib clinical data with CALAA-01, a targeted, polymer-based nanoparticle containing siRNA, Proc. Natl. Acad. Sci. U. S. A. 111 (2014) 11449–11454.
[23] J. Hrkach, D. Von Hoff, M.M. Ali, E. Andrianova, J. Auer, T. Campbell, D. De Witt, M. Figa, M. Figueiredo, A. Horhota, S. Low, K. McDonnell, E. Peeke, B. Retnarajan, A. Sabnis, E. Schnipper, J.J. Song, Y.H. Song, J. Summa, D. Tompsett, G. Troiano, T.V.G. Hoven, J. Wright, P. LoRusso, P.W. Kantoff, N.H. Bander, C. Sweeney, O.C. Farokhzad, R. Langer, S. Zale, Preclinical development and clinical translation of a PSMA-targeted docetaxel nanoparticle with a differentiated pharmacological profile, Sci. Transl. Med. 4 (2012) 128ra39.
[24] X. Gao, J. Zhao, G. Han, Y. Zhang, X. Dong, L. Cao, Q. Wang, H.M. Moulton, H.F. Yin, Effective dystrophin restoration by a novel muscle-homing peptide–morpholino conjugate in dystrophin-deficient mdx mice, Mol. Ther. 22 (2014) 1333–1341.
[25] L. Cao, G. Han, C. Lin, B. Gu, X. Gao, H.M. Moulton, Y. Seow, H.F. Yin, Fructose promotes uptake and activity of oligonucleotides with different chemistries in a context-dependent manner in mdx mice, Mol. Ther. - Nucleic Acids. 5 (2016) e329.
[26] X. Gao, N. Ran, X. Dong, B. Zuo, R. Yang, Q. Zhou, H.M. Moulton, Y. Seow, H.F. Yin, Anchor peptide captures, targets, and loads exosomes of diverse origins for diagnostics and therapy, Sci. Transl. Med. 10 (2018) eaat0195.
[27] F. Yue, P. Bi, C. Wang, J. Li, X. Liu, S. Kuang, Conditional loss of Pten in myogenic progenitors leads to postnatal skeletal muscle hypertrophy but age-dependent exhaustion of satellite cells, Cell Rep. 17 (2016) 2340–2353.
[28] M. Crone, J.K. Mah, Current and emerging therapies for Duchenne muscular dystrophy, Curr. Treat. Options Neurol. 20 (2018) 1795.
[29] C. Sun, C. Serra, G. Lee, K.R. Wagner, Stem cell-based therapies for Duchenne muscular dystrophy, Exp. Neurol. 323 (2020) 113086.
[30] A. Aartsma-Rus, A.M. Krieg, FDA approves Eteplirsen for Duchenne muscular dystrophy: the next chapter in the eteplirsen saga, Nucleic Acid Ther. 27 (2017) 1–3.
[31] Y.P. Li, Y.Y. Pei, X.Y. Zhang, Z.H. Gu, Z.H. Zhou, W.F. Yuan, J.J. Zhou, J.H. Zhu, X.J. Gao, PEGylated PLGA nanoparticles as protein carriers: synthesis, preparation and biodistribution in rats, J. Control. Release. 71 (2001) 203–211.
[32] F. Marcucci, F. Lefoulon, Active targeting with particulate drug carriers in tumor therapy: fundamentals and recent progress, Drug Discov. Today 9 (2004) 219–228.
[33] X. Yu, I. Trase, M. Ren, K. Duval, X. Guo, Z. Chen, Design of nanoparticle-based carriers for targeted drug delivery, J. Nanomater. 2016 (2016).
[34] N.A. Dumont, M.A. Rudnicki, Targeting muscle stem cell intrinsic defects to treat Duchenne muscular dystrophy, Npj Regen. Med. 1 (2016) 1–7.
[35] H. Yin, H.M. Moulton, C. Betts, Y. Seow, J. Boutilier, P.L. Iverson, M.J.A. Wood, A fusion peptide directs enhanced systemic dystrophin exon skipping and functional restoration in dystrophin-deficient mdx mice, Hum. Mol. Genet. 18 (2009) 4405–4414.
[36] Y. Seow, H. Yin, M.J.A. Wood, Identification of a novel muscle targeting peptide in mdx mice, Peptides 31 (2010) 1873–1877.
[37] K.M. Tsoi, S.A. Macparland, X.Z. Ma, V.N. Spetzler, J. Echeverri, B. Ouyang, S.M. Fadel, E.A. Sykes, N. Goldaracena, J.M. Kaths, J.B. Conneely, B.A. Alman, M. Selzner, M.A. Ostrowski, O.A. Adeyi, A. Zilman, I.D. McGilvray, W.C.W. Chan, Mechanism of hard-nanomaterial clearance by the liver, Nat. Mater. 15 (2016) 1212–1221.
[38] A.L. Arnett, P. Konieczny, J.N. Ramos, J. Hall, G. Odom, Z. Yablonka-Reuveni, J.R. Chamberlain, J.S. Chamberlain, Adeno-associated viral vectors do not efficiently target muscle satellite cells, Mol. Ther. - Methods Clin. Dev. 1 (2014) 14038.
[39] F. Yue, P. Bi, C. Wang, T. Shan, Y. Nie, T.L. Ratliff, T.P. Gavin, S. Kuang, Pten is necessary for the quiescence and maintenance of adult muscle stem cells, Nat. Commun. 8 (2017) 1–13.
[40] S. Shojaee, L.N. Chan, M. Buchner, V. Cazzaniga, K.N. Cosgun, H. Geng, Y.H. Qiu, M.D. Von Minden, T. Ernst, A. Hochhaus, G. Cazzaniga, A. Melnick, S.M. Kornblau, T.G. Graeber, H. Wu, H. Jumaa, M. Müschen, PTEN opposes negative selection and enables oncogenic transformation of pre-B cells, Nat. Med. 22 (2016) 379–387.
[41] X.G. Yang, X. Da Yang, L. Yuan, K. Wang, D.C. Crans, The permeability and cytotoxicity of insulin-mimetic vanadium compounds, Pharm. Res. 21 (2004) 1026–1033.
[42] S.C. Bodine, T.N. Stitt, M. Gonzalez, W.O. Kline, G.L. Stover, R. Bauerlein, E. Zlotchenko, A. Scrimgeour, J.C. Lawrence, D.J. Glass, G.D. Yancopoulos, Akt/mTOR pathway is a crucial regulator of skeletal muscle hypertrophy and can prevent muscle atrophy in vivo, Nat. Cell Biol. 3 (2001) 1014–1019.
[43] M.S. Alexander, J.C. Casar, N. Motohashi, N.M. Vieira, I. Eisenberg, J.L. Marshall, M.J. Gasperini, A. Lek, J.A. Myers, E.A. Estrella, P.B. Kang, F. Shapiro, F. Rahimov, G. Kawahara, J.J. Widrick, L.M. Kunkel, MicroRNA-486-dependent modulation of DOCK3/PTEN/AKT signaling pathways improves muscular dystrophy-associated symptoms, J. Clin. Invest. 124 (2014) 2651–2667.

Please cite this article as: D. Huang, F. Yue, J. Qiu et al., Polymeric nanoparticles functionalized with muscle-homing peptides for targeted delivery of phosphatase and tensin homolog inhibitor to skeletal muscle, Acta Biomaterialia, https://doi.org/10.1016/j.actbio.2020.10.009